Cement and Concrete Research 40 (2010) 1278–1289

Contents lists available at ScienceDirect

Cement and Concrete Research

journal homepage: http://ees.elsevier.com/CEMCON/default.asp

Assessment of the long-term stability of cementitious barriers of radioactive waste repositories by using digital-image-based microstructure generation and reactive transport modelling

Juan Manuel Galíndez [a,*], Jorge Molinero [b,1]

[a] Department of Agroforestal Engineering, University of Santiago de Compostela, Campus Universitario, 27002 Lugo, Spain
[b] Amphos XXI Consulting S.L., Passeig de García i Faria, 49-51, E08019 Barcelona, Spain

ARTICLE INFO

Article history:
Received 25 February 2009
Accepted 17 November 2009

Keywords:
Hydration (A)
Microstructure (B)
Durability (C)
Silica Fume (D)
Modeling (E)

ABSTRACT

Cement-based grout plays a significant role in the design and performance of nuclear waste repositories: used correctly, it can enhance their safety. However, the high water-to-binder ratios, which are required to meet the desired workability and injection ability at early age, lead to high porosity that may affect the durability of this material and undermine its long-term geochemical performance.

In this paper, a new methodology is presented in order to help the process of mix design which best meets the compromise between these two conflicting requirements. It involves the combined use of the computer programs CEMHYD3D for the generation of digital-image-based microstructures and CrunchFlow, for the reactive transport calculations affecting the materials so simulated. This approach is exemplified with two grout types, namely, the so-called Standard mix 5/5, used in the upper parts of the structure, and the "low-pH" P308B, to be injected at higher depths.

The results of the digital reconstruction of the mineralogical composition of the hardened paste are entirely logical, as the microstructures display high degrees of hydration, large porosities and low or nil contents of aluminium compounds.

Diffusion of solutes in the pore solution was considered to be the dominant transport process. A single scenario was studied for both mix designs and their performances were compared. The reactive transport model adequately reproduces the process of decalcification of the C–S–H and the precipitation of calcite, which is corroborated by empirical observations. It was found that the evolution of the deterioration process is sensitive to the chemical composition of groundwater, its effects being more severe when grout is set under continuous exposure to poorly mineralized groundwater. Results obtained appear to indicate that a correct conceptualization of the problem was accomplished and support the assumption that, in absence of more reliable empirical data, it might constitute a useful tool to estimate the durability of cement-based structures.

1. Introduction

Sealing of fractured bedrocks by means of the injection of cement-based grout is a standard procedure to enhance the compactness of the medium and reduce its permeability, thus precluding the spread of pollutants and minimizing groundwater inflow into tunnels. Under prolonged contact with groundwater, however, cement-based grout undergoes a slow, yet continuous degradation process which may undermine its integrity in the long-term. It is therefore apparent that the evaluation of the durability of cement-based grout is a relevant issue to be considered in the safety assessment of nuclear waste repositories.

The problem just set is complex as the selection of the grout mix design should also take into account the requirements of workability and injection ability. For the sake of illustration, an excerpt of a recent report on the subject [1] reads:

> 'The development of low-pH cementitious grout consisted of several tasks. First the potential systems were selected, based on the outcome of the earlier studies and on expert judgement, and the technical properties of some **two hundred recipes** (emphasis added) were tested. The most promising recipes were then selected for pH and leaching tests. Based on these results, the most promising recipes were tested in two small pilot field-tests in Finland.'

In fact, the question as to which mix is best regarding the objectives pursued remains nevertheless open, in spite of several mix designs

* Corresponding author.
E-mail address: juanmanuel.galindez@usc.es (J.M. Galíndez).
[1] Tel.: +34 93 583 05 00; fax: +34 93 307 59 28.

0008-8846/$ – see front matter © 2009 Elsevier Ltd. All rights reserved.
doi:10.1016/j.cemconres.2009.11.006

having been tested over recent years. Furthermore, as pointed out by Trotignon et al. [2], previous modelling works have not addressed the comparative evaluation of the performance of different types of concrete, or have only focused on Portland cement-based concrete.

In this paper, a methodological approach is presented to tackle this issue, which is expected to help narrow the range of the "ideal" mix design by evaluating in a simple and effective manner the long-term geochemical performance of digitally-generated cement-based grout microstructures. The digital simulation of the microstructure of the hardened cement paste represents a critical juncture of the analysis since, despite entailing a number of non-trivial assumptions, it provides a rational method to obtain the likely constitution of a grout wherever the conditions of hydration (and actually any data other than the volume fractions involved in the un-hydrated mixture) are uncertain. In other words, the present work is not intended to dissipate the incertitude connected to the actual evolution of the process of hydration under field conditions but, rather, to define reasonable starting points for subsequent modelling of degradation.

The results of the simulation of the microstructure of hardened cement paste are then linked to the evaluation of its long-term degradation under aggressive conditions. The estimated mineralogical and physical properties of the microstructure of cement-based grout are input into a reactive transport model set up in order to match the characteristics of the structure under analysis. In this case, a model was developed in an attempt to reproduce the degree of alteration undergone by a cylindrical grout specimen. Even though precedents of this approach exist in previous works [3–5], this field of research remains relatively unexplored, and it will serve well to illustrate some of the major concerns involved in the numerical simulation of concrete deterioration.

2. Materials

Two different mixtures have been analyzed in this work. As stated in [6], the mix design labelled as Standard grout mix 5/5 is an example of an injection grout for use in the upper sections of a tunnel under construction at Olkiluoto, Finland, whereas the P308B grout is a so-called "low-pH" grout which was developed to be injected at greater depths and was found to be one of the most promising ones for that purpose [7]. Mixes are listed in Table 1. Both include the sulphate-resistant low alkaline microcement Ultrafin 16 (a product manufactured by Cementa AB), which, thanks to its extremely finely ground especially selected clinker, has excellent penetration characteristics. Ultrafin 16 also complies with the low C_3A requirement for sulphate-resistant cement, in accordance with SS 13 42 04. C_3A content is normally restricted to 2% by weight.

Even though Ultrafin 16 is the cement positively used in the mixtures analyzed hereafter, in this work, an additional sensitivity analysis was carried out with respect to the particle size distribution of cement clinker, in order to evaluate its effect on the resulting microstructure of the hardened grout. To that aim, two additional microcements (namely Ultrafin 12 and Injektering 30) were studied. Ultrafin 16, Ultrafin 12 and Injektering 30 share the same chemical composition but have different particle size distributions. Their characteristic PSD curves were provided by manufacturers and are shown in Fig. 1. The chemical composition of Ultrafin 16 is, according to [8], the one given in Table 2, where all components are expressed in weight percentages.

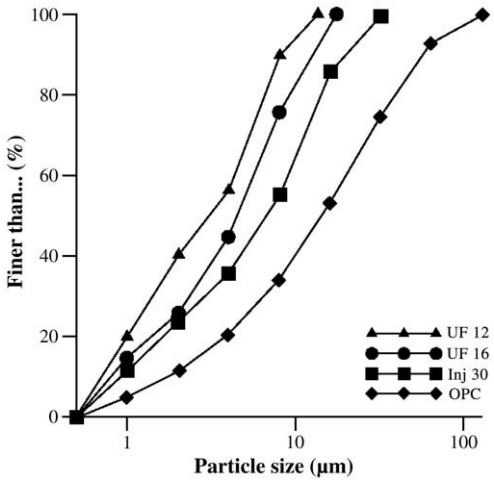

Fig. 1. Particle size distribution curves of different types of cement (product information provided by Cementa AB).

The lowering of pH of the pore solution is accomplished, in the case of P308B grout, by the larger addition of silica fume and has beneficial effects on the long-term safety because the pore water of the material is much less reactive towards the bentonite clay that surrounds the metal canisters of the waste repository. Silica fume was used as GroutAid, a silica-fume-based additive developed by Elkem Materials. The main feature of GroutAid is that its particles are extremely fine: a typical particle size distribution is shown in Fig. 2, where it is seen that more than 90% by weight is less than 1 μm. The microscopic particle size and pozzolanic reactivity of the so-called microsilica act to reduce bleeding and segregation, develop stronger and less permeable grout and increase durability and resistance to chemical attack.

In order to reduce the requirements of water, superplasticizer Mighty 150 (naphthalene sulphonate-based superplasticizer by Degussa, now BASF Construction Chemicals) was also added to the mixture. Its addition results in water reductions which amount to up to 30%.

3. Simulation of the microstructure of the cement-based materials

The tools provided by the Virtual Cement and Concrete Testing Laboratory (VCCTL; http://ciks.cbt.nist.gov) have been used in order to set up the initial state of cement grout. The main program of the VCCTL, namely CEMHYD3D, has been described previously [9] and was intensively tested in numerous applications [10–15].

The process of numerical generation of the final microstructure of the hardened grout proceeds in a series of steps consisting of: 1) the creation of the particle size distribution for both cement clinker and silica fume (when used); 2) the generation of the initial microstructure; 3) the distribution of cement phases; and 4) the simulation of hydration.

Table 1
Grout mixes to be used at ONKALO (After Holt, 2006 [6]).

Component	Standard grout mix 5/5 (kg)	P308B (kg)	Specific gravity	Standard grout mix 5/5 (dm^3)	P308B (dm^3)
Water	781.00	882.00	1.00	781.00	882.00
Ultrafin 16	664.00	372.00	3.20	207.50	116.25
Silica fume	117.00	256.00	2.20	53.18	116.36
Superplasticizer	21.90	25.30	–	–	–
Water/cement ratio	1.18	2.37			
Total	1583.90	1535.30	–	1041.68	1114.61

Table 2
Chemical composition of Ultrafin 16, main component of the low alkali grout.

Component	Weight percentage
CaO	64.80
SiO_2	22.30
Al_2O_3	3.40
Fe_2O_3	4.30
SO_3	2.40
Na_2O	–
Others	2.80

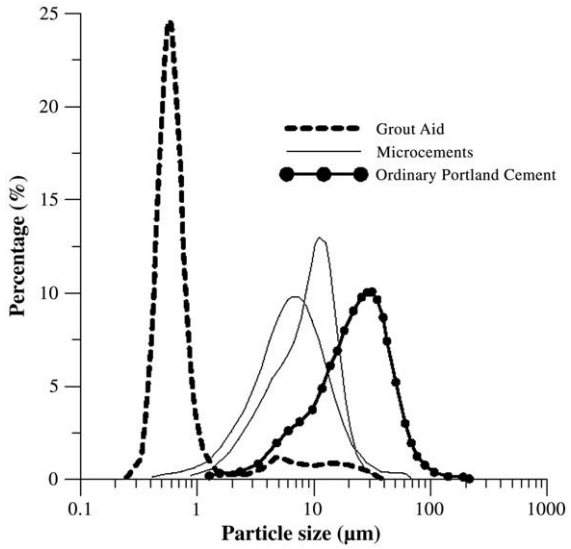

Fig. 2. Particle size distribution of silica fume compared to typical microcements and ordinary Portland cement (product information provided by Elkem Materials).

3.1. Creation of the particle size distribution

By creating a particle size distribution (i.e., the mass fraction expressed as a function of particle diameter) the number of cement particles of each diameter to be placed in a starting three-dimensional microstructure is specified. Two different input (PSD) files were generated, one corresponding to the anhydrous cement itself, and the other to the silica fume added, on the basis of data shown in Figs. 1 and 2, respectively. As said earlier, the process was repeated three times (one each for Ultrafin 16, Ultrafin 12 and Injektering 30) for each grout recipe (either Standard 5/5 or P308B), resulting in a total of six different microstructures of hardened grout.

3.2. Generation of the initial microstructure

The number of pixels of a three-dimensional image of the mixture which is assigned to each of its solid compounds was calculated from the volumes of each component shown in Table 1, and corrected in order to match the prescribed water-to-cement ratio for each mix design.

A three-dimensional cement-based grout mixture microstructure is then generated, consisting of the sum of the selected compounds in water, namely cement clinker and silica fume, with their respective particle size distribution. The influence of the superplasticizer can also be modelled in a two-fold way: by enabling the flocculation into several flocs; and by "dispersing" the particles into the initial microstructure. Details of the process can be found in the User's Guide of CEMHYD3D [16].

3.3. Distribution of the cement phases

Since the microstructure image created by the preceding steps is composed of single-phase particles only, once the initial arrangement of generic anhydrous particles in water has been created, the four major phases of cement clinker (i.e., C_3S, C_2S, C_3A and C_4AF) should be distributed amongst the cement particles.

Based on the data shown in Table 2, a Bogue calculation was used to determine the major phases present in the clinker (Table 3).

Ideally, the three-dimensional microstructure image is filtered using two-point correlation functions measured on the actual two-dimensional SEM (Scanning Electron Microscopy) images of the cement used. This is not possible in this case, for no SEM images of Ultrafin 16 clinker are available. Instead, the assumption was made that similar results would be obtained by distributing the major anhydrous cement phases according to the two-dimensional pattern described by a cement clinker whose composition matched closely that of Ultrafin 16, as listed in Table 3. That cement is found in the VCCTL database under the label "cementhoc", attributed to Danish white (low aluminate) cement. A detailed description on the process to obtain the digital images such as the one on the picture can be found in [17].

Table 3
Mineralogical composition of the cement clinker for Ultrafin 16.

Anhydrous compound*	Volume percentage
C_3S	70.46
C_2S	15.42
C_3A	1.98
C_4AF	12.14

* C_3S = tricalcium silicate; C_2S = dicalcium silicate; C_3A = tricalcium aluminate; C_4AF = tetracalcium ferrite aluminate.

Table 4
Calculated volume fractions (%) by the CEMHYD3D software for every mix design and cement particle size distribution.

Component[1]	Standard grout mix 5/5			P308B		
	UF 12	UF 16	Inj 30	UF 12	UF 16	Inj 30
Porosity	45.456	45.757	45.996	57.026	55.647	57.659
C_3S	0.000	0.001	0.008	0.000	0.011	0.005
C_2S	0.011	0.170	0.311	0.227	0.000	0.493
C_3A	0.000	0.000	0.000	0.000	0.000	4.742
C_4AF	0.000	0.000	0.000	0.000	0.000	0.038
Silica fume	0.458	0.607	0.639	4.547	3.622	0.029
$Ca(OH)_2$	3.637	3.836	3.903	0.001	0.031	0.614
C–S–H	29.402	29.164	28.347	0.021	0.003	0.003
C_3AH_6	1.173	1.177	1.177	0.611	0.000	0.000
FH_3	0.005	0.006	0.005	0.002	0.000	0.000
PozzC–S–H	19.856	19.282	19.615	37.566	40.686	36.417

[1] C–S–H = calcium silicate hydrates ($C_{1.7}SH_4$); FH_3 = iron hydroxide; PozzC–S–H = Pozzolanic calcium silicate hydrates ($C_{1.1}SH_{3.9}$).

3.4. Simulation of the hydration

Once the anhydrous mixture was determined, the simulation of the hydration process was performed by means of CEMHYD3D. A non-trivial assumption was made in this respect, for the conditions to which cement-based grout is subjected after injection differ considerably from the controlled conditions the program was intended to reproduce. In fact, whereas the latter can be set to be either saturated or sealed, and either adiabatic, isothermal or temperature-programmed for a given period of time (for the present case, hydration was assumed to progress under saturated conditions and a constant temperature of 25 °C), in-situ temperature and humidity may change during construction periods, thus altering the rate of hydration and increasing the risks of drying shrinkage, and the potential for cracking, due to a higher rate of evaporation from the fresh grout. Furthermore, grout is very sensitive and somewhat weak during its early ages and vibrations during excavation and construction can upset the quality of grouting and of bond in fissures; this

Table 5
Volume fractions as input into the reactive transport model. The cases studied are highlighted.

Component	Standard grout mix 5/5	P308B
Porosity	45.757	55.647
SiO_2(am)	0.607	3.622
$Ca(OH)_2$	3.836	0.031
$C_{1.8}$–S–H	29.335	0.014
$C_{1.1}$–S–H	19.282	40.686
$C_{0.8}$–S–H	0.000	0.000

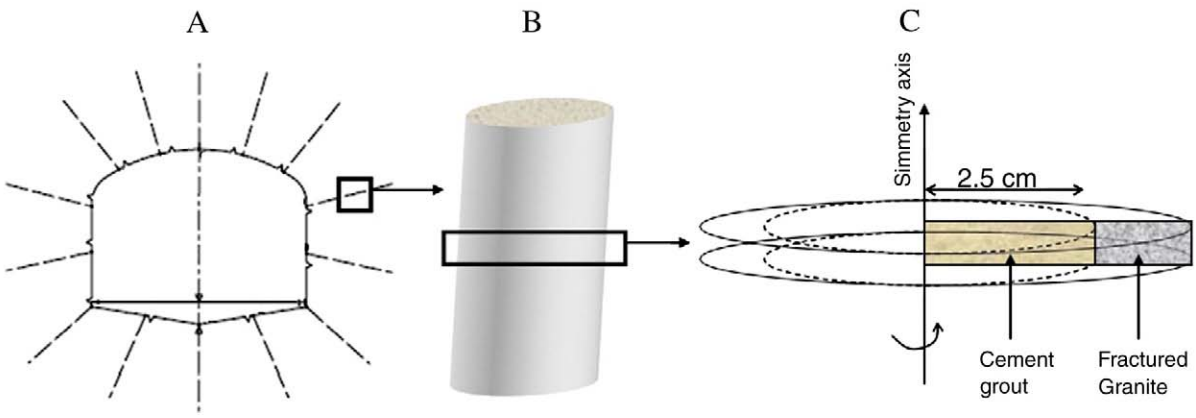

Fig. 3. Scheme of the model.

could result in additional pathways for future leaching or deterioration. As a consequence, the hypothesis was made that the microstructural characteristics of the hydrated paste would be roughly the same regardless of the conditions of curing if the degree of hydration was high. Further research might be needed on this topic.

3.5. Results

Table 4 shows the obtained outputs of CEMHYD3D after a period of hydration of more than 100 days, displaying the volume fraction distribution of the components of the hydrated microstructure of cement-based grout for the simulations carried out for the 6 cases resulting from the combinations between 2 cement–grout recipes and 3 particle size distributions. The extremely low volume fractions obtained for the anhydrous components of cement denote that the degree of hydration reached is close to 100% for all cases. It is also apparent that the addition of silica fume results in a large decrease of the volume fraction of portlandite ($Ca(OH)_2$), absent for mix P308B.

The higher water-to-binder ratio (see Table 1) is reflected in the higher porosity of the mix design P308B. Even though volume fractions assigned to each mineral (and, therefore, also to porosity) vary considerably as a function of the mix design considered, the influence of the particle size distribution of cement clinker is of lesser relevance. Yet, simulations are consistent, as finer clinker particles are associated with higher degrees of hydration and, therefore, to smaller porosities. It is also worth pointing out the low content of aluminium compounds remaining, to which both the use of sulphate-resistant cement and the addition of silica fume have contributed.

The volume fractions obtained were regrouped in order to meet the requirements of the future reactive transport model that will be used to simulate the cement degradation process. Some hypotheses were made in the process: firstly, the anhydrous calcium compounds remaining were grouped together with calcium silicate hydrates. This entails the assumption that anhydrous compounds, initially preserved from the contact with water by surrounding hydrated cement, will be exposed as soon as outer layers dissolve, thus turning into hydrated products themselves.

Furthermore, katoite ($Ca_3Al_2(SiO_4)_{3-x}(OH^-)_{4x}$, with $x = 1.5$ to 3) and FH_3 were not considered in the initial microstructures. In fact, aluminium system is not simulated in the current version of the reactive transport model for grout degradation since the amount of aluminium phases in the hydrated cement grouts considered in this work is very small. These considerations notwithstanding, neglecting aluminium and iron compounds responds to an attempt to simplify the reactive transport model rather than to the acknowledgment of their actual relevance.

Table 6
Chemical composition of boundary water: Borehole KLX02 at a depth of −452.5 m.a.s.l. [24].

Component	Concentration (mol/L)	Concentration (mol/L) (see Section 4)
pH	7.8	7.8
$SiO_{2(aq)}$	1.43E-04	1.43E-04
Na^+	1.70E-02	1.70E-02
K^+	9.64E-05	9.64E-05
Ca^{2+}	3.30E-03	3.30E-03
Mg^{2+}	4.19E-04	4.19E-04
HCO_3^-	2.14E-03	2.14E-04
SO_4^{2-}	1.51E-03	1.51E-03

Table 7
Hydrogeochemical reactions considered in the reactive transport model.

Homogeneous hydrogeochemical reactions	Log *K*	
$H^+ + OH^- \leftrightarrow H_2O$	+13.9951	
$CaHCO_3^+ \leftrightarrow Ca^{2+} + HCO_3^-$	−1.0467	
$CaSO_{4(aq)} \leftrightarrow Ca^{2+} + SO4^{2-}$	−2.1111	
$NaHCO_{3(aq)} \leftrightarrow HCO_3^- + Na^+$	−0.1541	
$NaSO_4^- \leftrightarrow Na^+ + SO_4^{2-}$	−0.8200	
$NaCO_3^- \leftrightarrow CO_3^{2-} + Na^+$	−0.5144	
$NaOH_{(aq)} + H^+ \leftrightarrow H_2O + Na^+$	+14.1800	
$NaHSiO_{3(aq)} + H^+ \leftrightarrow H_2O + Na^+ + SiO_{2(aq)}$	+8.3040	
$KOH_{(aq)} + H^+ \leftrightarrow H_2O + K^+$	+14.4600	
$KSO_4^- \leftrightarrow K^+ + SO_4^{2-}$	−0.8796	
$CO_{2(aq)} + H_2O \leftrightarrow H^+ + HCO_3^-$	−6.3447	
$CO_3^{2-} + H^+ \leftrightarrow HCO_3^-$	+10.3288	
$CaCO_{3(aq)} + H^+ \leftrightarrow Ca^{2+} + HCO_3^-$	+7.0017	
$CaOH^+ + H^+ \leftrightarrow Ca^{2+} + H_2O$	+12.8500	
$H_2SO_{4(aq)} \leftrightarrow SO_4^{2-} + 2H^+$	+1.0200	
$HSO_4^- \leftrightarrow H^+ + SO_4^{2-}$	−1.9791	
$H_2SiO_4^{2-} + 2H^+ \leftrightarrow SiO_{2(aq)} + 2H_2O$	+22.9116	
$H_4(H_2SiO_4)_4^{4-} + 4H^+ \leftrightarrow 4SiO_{2(aq)} + 8H_2O$	+35.9400	
$H_6(H_2SiO_4)_4^{2-} + 2H^+ \leftrightarrow 4SiO_{2(aq)} + 8H_2O$	+13.6400	
$HSiO_3^- + H^+ \leftrightarrow SiO_{2(aq)} + H_2O$	+9.9525	
$KHSO_{4(aq)} + H^+ \leftrightarrow H^+ + K^+ + SO_4^{2-} +$	−0.8136	
Mineral processes	**Log *K***	**Molar volume (cm^3/mol)**
$Ca(OH)_2 + 2H^+ \leftrightarrow Ca^{2+} + 2H_2O$	+22.5552	33.056
$C_{0.8}$–S–H + $1.6H^+ \leftrightarrow 1.8H_2O + SiO_{2(aq)} + 0.8Ca^{2+}$	+10.8614*	101.800
$C_{1.1}$–S–H + $2.2H^+ \leftrightarrow 2.1H_2O + SiO_{2(aq)} + 1.1Ca^{2+}$	+16.5014*	101.800
$C_{1.8}$–S–H + $3.6H^+ \leftrightarrow 2.8H_2O + SiO_{2(aq)} + 1.8Ca^{2+}$	+32.4814*	108.000
$SiO_{2(s)} \leftrightarrow SiO_{2(aq)}$	−2.7136	29.000
$CaCO_{3(s)} + H^+ \leftrightarrow Ca^{2+} + HCO_3^-$	+1.8487	36.934

* The solubility product was deduced from data reported by Stronach and Glasser [25] and Westall et al. [26].

At this point, it is also worth noting that, because of C–S–H comprising a wide variety of phases, ranging from cryptocrystalline to nearly amorphous and variable solid solution compositions of different Ca/Si ratios, their thermodynamic behaviour is extremely complex. A remarkably large amount of effort has been devoted in recent years to the characterization of C–S–H. Nevertheless, as was opportunely pointed out in [18], a phenomenological framework is lacking which is able to synthesize the current knowledge of C–S–H in terms of the variations of significant parameters such as the calcium-to-silica ratio, the silicate structure and the contents of Si–OH and Ca–OH. Moreover, such factors as the composition of cement, the water-to-cement ratio, the curing temperature, the degree of hydration, and the presence of chemical and mineral admixtures add to the inherent complexity of the task in question.

A plethora of modelling techniques was developed as a consequence, the description of which is beyond the scope of this work and can be found elsewhere [19]. One of them consists of considering C–S–H to be an assemblage of different mineral phases, characterized by diverse calcium-to-silica ratios and solubility products. This approach has already been taken in previous investigations [5,20] and it involves a simplified representation of the actual thermodynamic behaviour of C–S–H.

In Table 5, the volume fractions considered for every case, arranged according to the assumptions made above concerning the use of either cement (Ultrafin 12, Ultrafin 16 or Injektering 30), are listed. In view that the composition of the hydrated paste is not remarkably sensitive to the size distribution curves of cement clinker, only one microstructure of each recipe (the one corresponding to Ultrafin 16 particle size distribution) has been considered for subsequent reactive transport modelling of grout degradation.

4. Reactive transport modelling

4.1. Conceptual model for the degradation of cement-based grout

Under the assumption of local chemical equilibrium, which has proved to hold for most practical cases involving diffusion of ions in cementitious materials [21], the reactive transport problem may be formulated in terms of a mixed set of equations, comprising both algebraic and partial differential equations. In view of the intrinsic microstructural complexity of the hardened cement paste, the scale over which the integration of differential equations is performed becomes a matter of concern. In this respect, paths have diverged. On the one hand, the problem might indeed be solved at a microscopic scale, which implies the digital simulation of the pore structure of cement systems based, for instance, on microstructural information obtained by means of experimental procedures (e.g., mercury intrusion porosimetry). On the other hand, a Representative Elementary Volume (REV) might be defined, such that its properties can properly describe the heterogeneous material which is composed of. Using this method the most relevant variables are averaged over such volume, thus relaxing the need for detailed knowledge of the microstructure of the material. Such average properties can easily be measured in practice. The validity of this approach, often referred to as the homogenization technique, lies on the adequacy of the definition of the REV for the problem of interest. This is attained when, regardless of its location within the domain, the REV always contains persistent volumes of solid and voids [22]. This latter approach was the one taken in this work for the resolution of the reactive transport problem. Indeed, in this case, the size of the REV is given by the three-

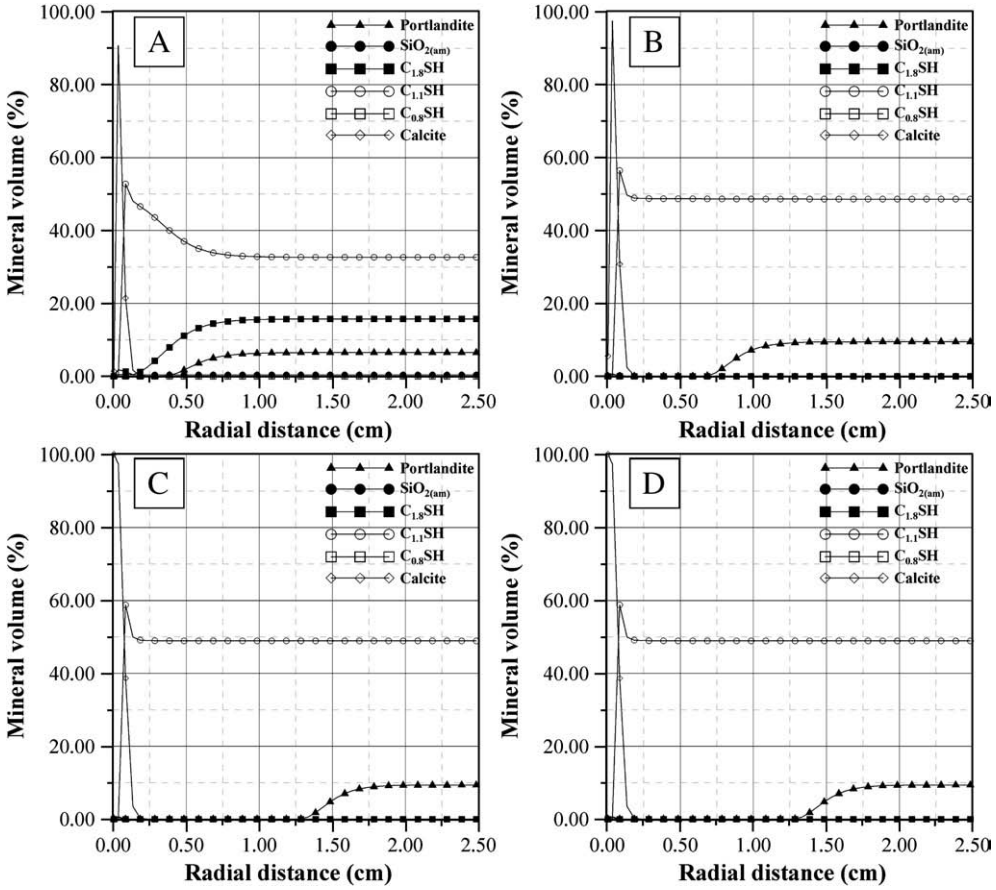

Fig. 4. Mineral constitution of Standard 5/5 injection grout after (A) 0.25 year, (B) 1 year, (C) 50 years and (D) 1000 years.

dimensional picture obtained by the digital-image-based cement hydration modelling software, i.e., 100 μm × 100 μm × 100 μm [23].

4.2. Description of the scenario under study

A model was developed which is intended to simulate the degradation of a long drill hole for grout injection in fractured granite, as the one depicted in Fig. 3, for a typical cross-section of a tunnel (Fig. 3A). If the hole is long enough, the degradation induced by leaching would progress in a radial direction from the surface towards its centre, i.e., the assumption of axisymmetry would hold, and a one-dimensional axisymmetric model would be sufficient. Fig. 3B shows a slice of the cylindrical drill hole (filled with cement-based grout up to 2.50 cm from the central axis) surrounded by a thick granite layer. The scheme considered for the simulations on which degradation will be analyzed, is depicted in Fig. 3C.

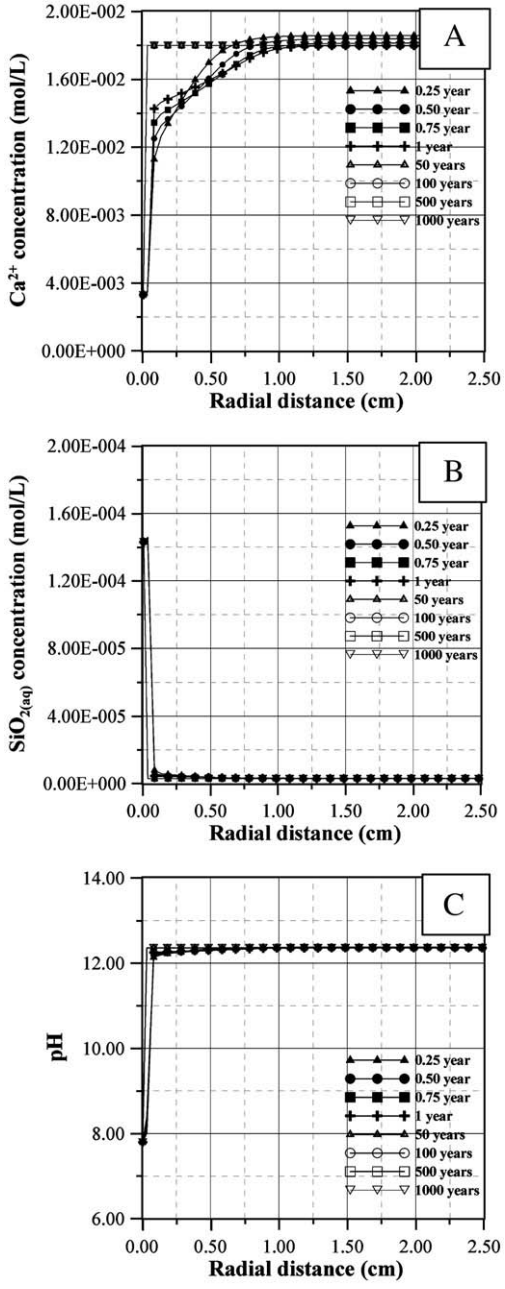

Fig. 5. Concentration of (A) calcium and (B) silica, and (C) pH in the pore water of the Standard 5/5 injection grout specimen.

The numerical resolution of the problem was based on a finite-element scheme. Grout was discretized into a one-dimensional mesh consisting of 50 elements with a uniform length of 0.05 cm.

In a worst case scenario, interstitial granite water might be constantly renewed through the fractures of the bedrock and, as a consequence, the hyperalkaline front spreading away from the grout specimen will dilute into the large volume of groundwater. Such scenario can be represented by fixing the chemical composition of water at the outer surface of grout to equal the chemical composition of the surrounding rock (i.e., imposing a boundary condition of the Dirichlet type). Some aspects of the simulation must then be acknowledged:

1) The model entails the assumption that the volume of grout is not relevant to induce a significant hyperalkaline plume in the surroundings.
2) The conditions are aggressive for grout (similar boundary conditions were applied in an analogous problem presented in [2]) but hardly critical for its surroundings, since their likely sphere of influence is constrained.

Granite was assumed to be unreactive. The chemical composition of the boundary water was assumed to match a water sample of the Laxemar area (Sweden) at a depth of 500 m, a characteristic depth often considered for a nuclear waste repository (see Table 6).

A total of 21 homogeneous hydrogeochemical reactions and 6 mineral processes were considered in the modelling and are listed in Table 7.

Molar volumes of C–S–H species are taken from [23].

4.3. Numerical tools

The numerical modelling tool CrunchFlow is a computer program for multicomponent reactive transport in porous media. CrunchFlow is an enhanced version of the GIMRT/OS3D package [27,28] which can be used for reactive transport problems of arbitrary complexity and size (i.e., there is no a priori restriction on the number of species or reactions considered). Some of its main features include the simulation of advective, dispersive, and diffusive transport in up to two dimension using the global implicit (GIMRT) option; non-isothermal transport and reaction; multicomponent aqueous complexation; kinetically-controlled mineral precipitation and dissolution; and reaction-induced porosity and permeability feedback to both diffusion and flow. The reader is referred to the User's Guide of CrunchFlow [29] for a more comprehensive discussion of the conceptual and mathematical foundations of reactive transport models.

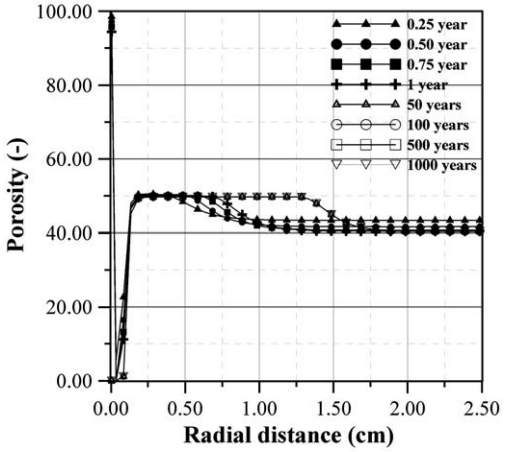

Fig. 6. Evolution of porosity with time for the Standard 5/5 injection grout specimen.

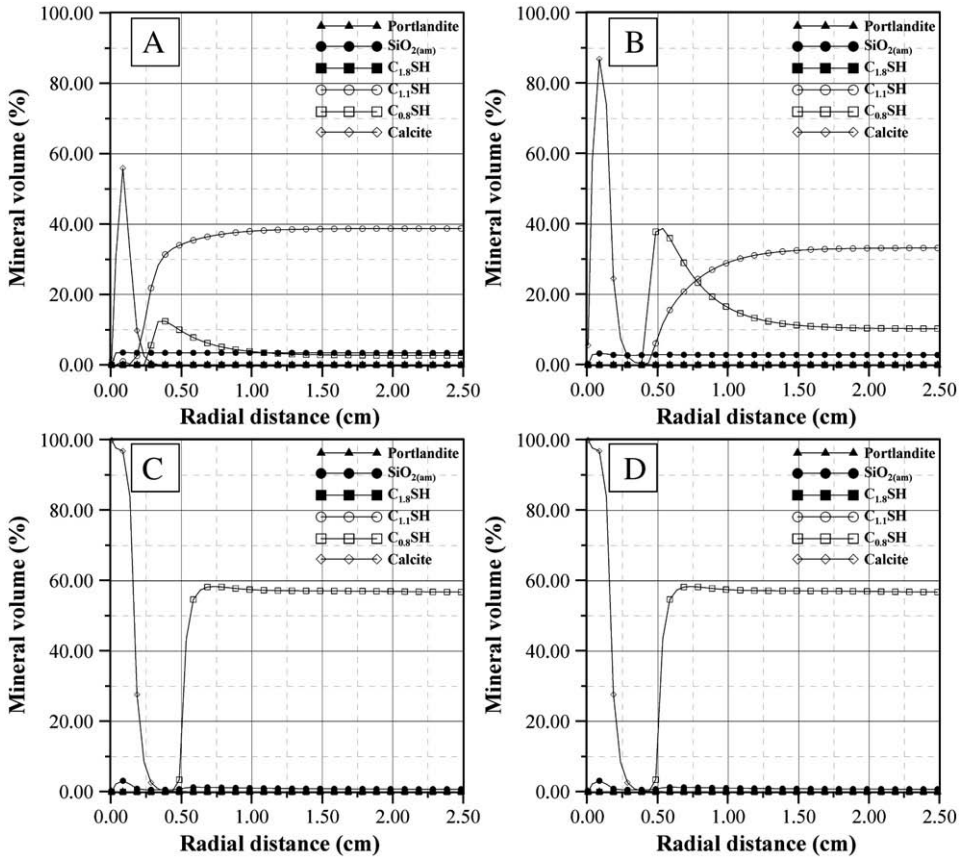

Fig. 7. Mineral constitution of P308B injection grout after (A) 0.25 year, (B) 1 year, (C) 50 years and (D) 1000 years.

For the sake of simplification, physical adsorption of ionic species at the mineral phases and electrostatic effects were neglected.

CrunchFlow makes use of the relationship given in Eq. (1) [30]:

$$D_{\text{eff}} = \frac{\Phi^m}{F} D_0 \tag{1}$$

Where D_{eff} denotes the effective diffusion coefficient; $D_0 = 2.20\text{E-}09$ m^2/s, the diffusion coefficient in pure water; and the parameters F and m are respectively the formation factor and the cementation exponent.

Research on computer-simulated microstructures of cement-based materials, though, has shown that a more precise expression for the diffusion coefficient would be [31]:

$$D_{\text{eff}} = [0.001 + 0.07\phi^2 + 1.8H(\phi-\phi_c)(\phi-\phi_c)^2]D_0 \tag{2}$$

Where $\phi_c = 0.18$ represents the critical capillary porosity of the material; and $H(\phi_f - \phi_c)$ is the Heavyside function.

The parameters F and m were therefore estimated by fitting the curve ϕ vs. D_{eff} obtained with Eq. (1) to the one described by Eq. (2), for the range of porosities of the grout under study. The values calculated in this manner were $m = 2.55$ and $F = 0.78$.

4.4. Results

4.4.1. Case I: Standard grout mix 5/5

One feature of the evolution of the degradation front for the grout specimen made up of Standard grout mix 5/5 (Fig. 4) is the complete depletion of portlandite from a 1.25-cm-thick superficial layer at approximately 50 years of simulation. This is consistent with the widely accepted observation that portlandite is the first solid species to totally dissolve [5,32,33].

On the other hand, the process of decalcification of C–S–H (which is denoted by the gradual shift of their calcium-to-silica ratio from high values towards lower ones) is reproduced by the increase of the relative proportion of $C_{1.1}$–S–H in detriment of $C_{1.8}$–S–H, induced by the simultaneous dissolution of $C_{1.8}$–S–H and the precipitation of $C_{1.1}$–S–H. This phenomenon is particularly evident in the proximity of the exposed surface, but it also takes place in inner regions of the grout specimen. The process of decalcification of C–S–H is, however, not entirely detrimental for the integrity of the grout specimen, since the emerging $C_{1.1}$–S–H appears to be significantly more stable than $C_{1.8}$–S–H under the new geochemical conditions of the pore solution.

The progress of deterioration is therefore not entirely related to the advance of a sharp front but, rather, to the gradual alteration of the governing equilibrium between a changing pore solution and the reacting solid phase, which undergoes the dissolution of the richer calcium-containing mineral phases of grout. Another noteworthy feature of degradation is the precipitation of calcite on the exposed surface of the specimen (arising from the presence of bicarbonates in the surrounding groundwater, in combination with the calcium ions which are released outwards from the core of the specimen), which tends to fill the capillary pores. This is corroborated by empirical observations reported in previous works [34,35]. The clogging of the pore network also has a beneficial effect on the lowering of the diffusion rate and, as a consequence, on the decrease of the rate of advance of the front of dissolution of portlandite. This holds true to such extent that after less than 50 years, the surface of the specimen is completely sealed, hindering the further advance of deterioration. The snapshots at simulation times of 50 years and later suggest that a new equilibrium stage was reached where dissolution of portlandite has halted its progress, and no further decalcification of C–S–H is seen.

In strong agreement with observations made by [5] for ordinary Portland cements, calcium concentration rises sharply up to 1.80E-

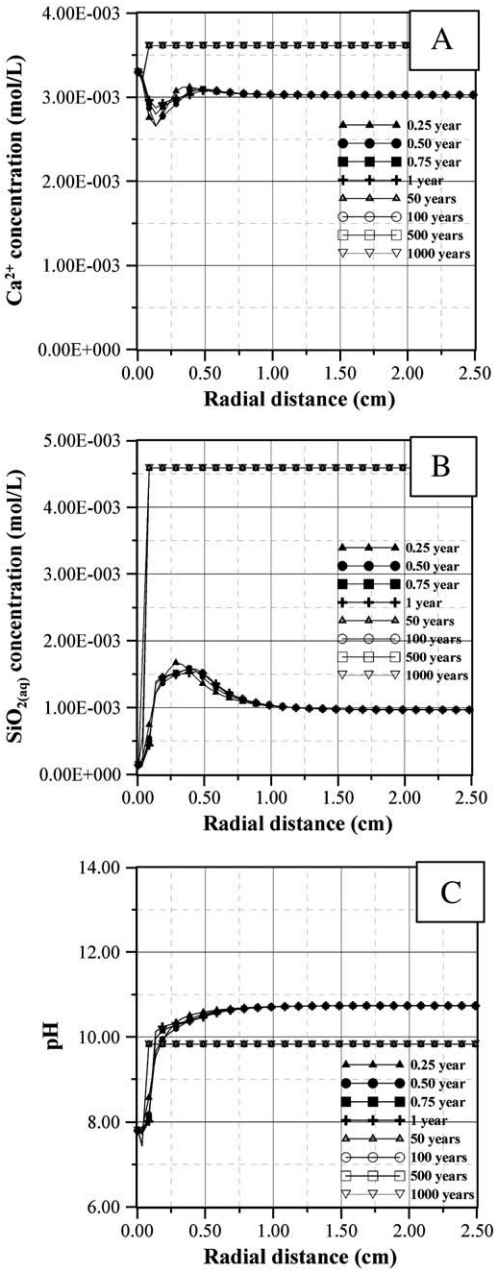

Fig. 8. Concentration of (A) calcium and (B) silica, and (C) pH in the pore water of the P308B injection grout specimen.

02 mol/L after less than a year of exposure (Fig. 5A). In that work, this process is attributed to the depletion of alkali ions from the pore solution, due to diffusive fluxes, and the subsequent replacement by calcium ions, released from the cement paste through portlandite dissolution. The decalcification of C–S–H adds to this effect. Whereas pH stays relatively stable at 12.35 (Fig. 5C), at later stages of deterioration, calcium ions are leached outwards due to the concentration gradient which is established between the pore solution and the boundary groundwater. This phenomenon continues as long as there is some pore space remaining connecting the pore solution to the environment, i.e., until the "barrier" of calcite which forms on the surface of the specimen does not hinder the transport of species. By sealing the pores, calcite isolates the pore solution from its environment, and therefore enables calcium to increase uniformly along the entire depth of the specimen.

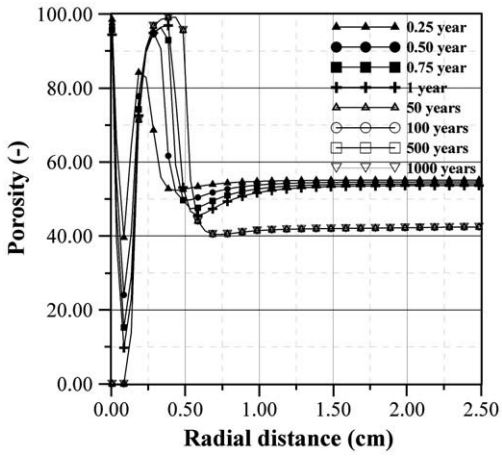

Fig. 9. Evolution of porosity with time for the P308B injection grout specimen.

Fig. 6 shows the evolution of the porosity in successive profiles obtained after different times of simulation. It is apparent that the increase of the porosity is related to a great extent to the dissolution of portlandite, which progresses towards the centre of the grout specimen, and the precipitation of a large amount of calcite on the exposed surface, which tends to seal the pore network. After 1000 years of simulation, however, it is seen that the most dramatic effects of deterioration are confined to 1.5 cm from the exposed surface. The core of the specimen remains virtually unaltered.

4.4.2. Case II: P308B grout mix

The results of the simulation of the deterioration of P308B grout are shown in Fig. 7, in terms of the evolution of the mineral phases. As can be observed, in absence of portlandite, the process of deterioration is reflected mainly on the decalcification of C–S–H. It is apparent that the behaviour of the solid phase in response to the changes that the entry of external groundwater induces on the geochemical properties of the pore solution is two-fold. On the one hand, the process of decalcification (i.e., the dissolution of $C_{1.1}$–S–H and the precipitation of $C_{0.8}$–S–H) leads to almost the complete disintegration of the material in the vicinity of the exposed surface. On the other hand, the process of decalcification involves the evolution of the C–S–H from calcium-richer, more soluble phases towards more stable compounds under low-pH conditions. As a consequence, the front of deterioration advances at a low rate and the most dramatic effects of degradation are confined to less than 0.5 cm after 1000 years. Moreover, the higher amount of $C_{0.8}$–S–H precipitated induces the decrease of the porosity, thus further hindering the progress of degradation. As can be seen, calcite tends to fill the space of the original position of the surface of the specimen and stays isolated from the core of the specimen. Whether this is mechanically possible remains an open question to which it is not possible to give a definite answer with the results obtained at hand. However, a rational analysis based upon physical, rather than numerical, considerations would enable to hypothesize that calcite should precipitate around the actual surface of the solid, wherever its position, around which the initial crystals may nucleate. In that scenario, the trend observed in the sequence shown in Fig. 7 allows one to envisage a final less porous material made up of a large amount of C–S–H with a calcium-to-silica ratio of Ca/Si = 0.8, protected by a relatively thick layer of calcite.

The properties of the P308B cement and, in general, of low-pH cement grouts become apparent from Fig. 8. The pore solution in contact with such grout is characterized by lower contents of calcium and higher concentrations of silica with respect to Ordinary Portland cements. The numerical simulations also reproduce the significantly lower value of pH (Fig. 8C) obtained as a consequence of the addition of silica fume into the dry mixture. As in the previous case, the barrier

of calcite formed on the surface of the specimen shields the pore solution from the environment. The pH of the pore solution drops then down to approximately 9.8 once the equilibrium stage is attained.

The porosity of the grout specimen undergoes a dramatic increase near the surface, which virtually leads to the disintegration of the material (Fig. 9). As discussed above, the transformation of $C_{1.1}$–S–H into larger quantities $C_{0.8}$–S–H induces the decrease of the porosity in inner regions of the specimen, thus preventing the disintegration from advancing inwards. The associated decrease of the diffusion rate, along with the formation of a protective layer of calcite on the surface and the lower solubility of $C_{0.8}$–S–H, eventually settle into a state of pseudo-equilibrium at a certain distance from the exposed surface safeguarding the integrity of the core of the specimen.

5. Testing the hydrochemical boundary condition

After the construction of the tunnel, the composition of groundwater at high depths (which, under undisturbed conditions is well known and might remain essentially constant) may undergo substantial variations as a consequence of different types of water flowing towards the tunnel as if towards a sink and mixing with deep groundwater. Given that the most suitable locations for deposit tunnels that are currently under consideration are generally to be found in coastal areas, different mixings between fresh waters of meteoric origin, marine waters and deep brines are possible at the depth of the tunnel. In turn, the actual composition of the boundary water determines the rate of advance of the front of degradation. In view of this, additional simulations were performed in order to get a notion of the sensitivity of the results with respect to the chemical composition of groundwater and, in particular, with respect to the content of bicarbonate, which was found to dampen the rate of degradation by contributing to the formation of calcite. Such sensitivity analyses might prove fruitful in estimating the range over which the actual rate of degradation can vary and, in particular, the maximum values that can occur. The additional simulations were carried out for both Standard 5/5 cement and P308B cement grout specimens exposed to a boundary water whose chemical composition is described in the third column of Table 6. Its main feature, with respect to the one of the reference cases, is that the content of HCO_3^- is one order of magnitude lower, which may be due to a greater contribution of meteoric water.

5.1. Case I: Standard 5/5 cement

As can be observed (Fig. 10), the effects of the relative lack of bicarbonate in groundwater has deleterious effects on grout since, by preventing the formation of a calcite "barrier" (although calcite does precipitate, it does not seal the pores tightly), it accelerates the processes of dissolution of portlandite and the decalcification of C–S–H. Indeed, after less than 50 years of exposure, portlandite is completely exhausted and the remaining fraction of C–S–H recedes approximately 1 cm from the initial position of the surface. Towards the inner regions of the specimen, the effects of degradation are seen as a larger proportion of $C_{0.8}$–S–H in the solid phase, which reflects a higher degree of decalcification. The process appears to be of an unstable nature since, apart from the precipitation of calcite, the lower solubility of $C_{0.8}$–S–H, and their dampening effect on the rate of degradation, there are no signs of a new equilibrium state. In other words, the deterioration would progress, though at lower rates, indefinitely.

Fig. 11 shows the gradual decrease that affects the concentration of calcium at earlier simulation times, due to the diffusive fluxes induced by the concentration gradient between the boundary and the pore waters. After 50 years of simulation, a concentration of approximately 4E-03 mol/L is reached, which is comparable to that observed in Fig. 8,

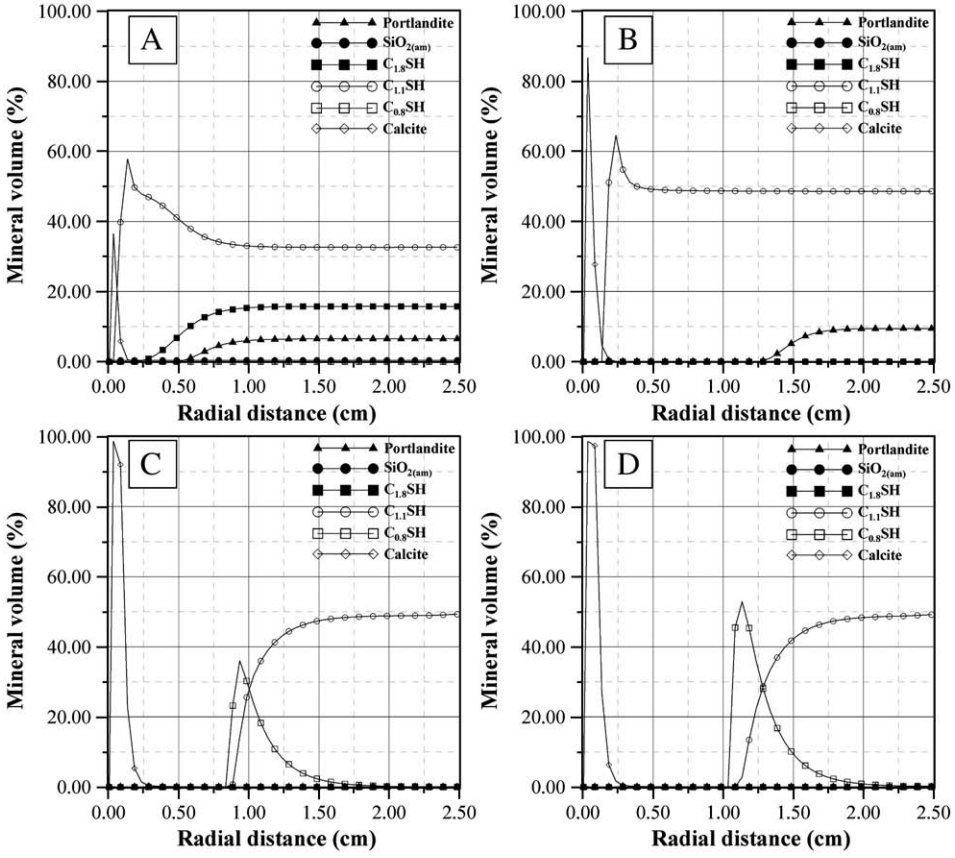

Fig. 10. Mineral constitution of Standard 5/5 injection grout after (A) 0.25 year, (B) 1 year, (C) 50 years and (D) 1000 years.

and in accordance with the prominence of C–S–H phases with lower Ca/Si ratios that remain. The evolution of pH (Fig. 11) follows a similar pattern: the typically high value of 12.35 drops down to 10.7 after 50 years of exposure.

As said above, in the present case, degradation progresses as a sharp front, due to the dissolution of C–S–H and the steep increase of the porosity, up to nearly 100% (Fig. 12). Distinct from the reference case (Case I), as well as the changes in the microstructure of grout, the most noteworthy effect of deterioration is the reduction of the effective diameter of the grout specimen, by disintegration of the outer solid layers.

5.2. Case II: P308B cement

As Fig. 13 shows, the durability of grout might be dramatically damaged by the lower bicarbonate in groundwater. Indeed, the process of degradation is accelerated to such extent that the grout specimen is completely disintegrated after a few years (less than 50) of exposure.

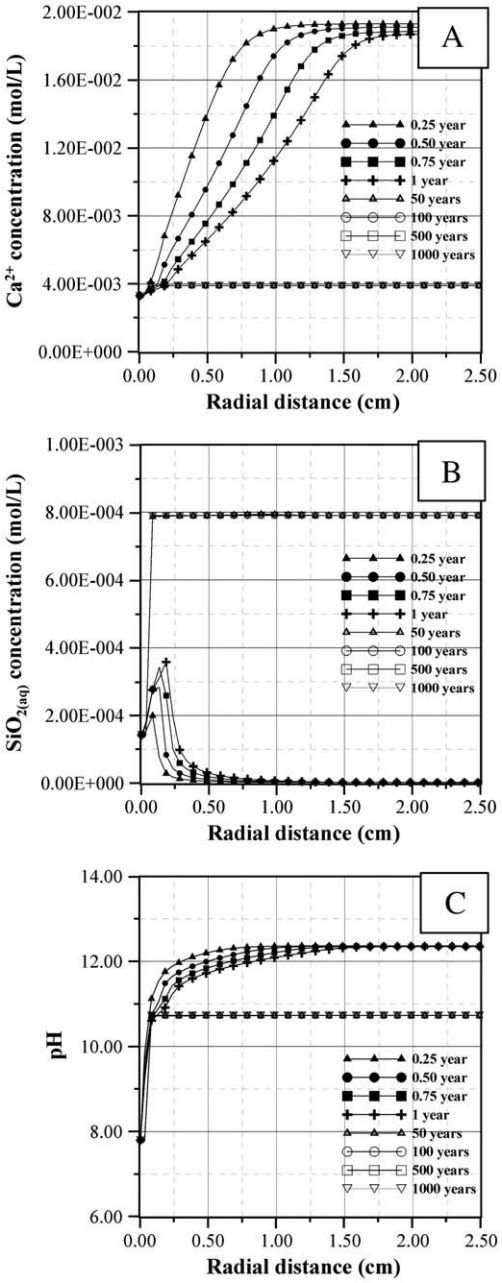

Fig. 11. Concentration of (A) calcium and (B) silica, and (C) pH in the pore water of the Standard 5/5 injection grout specimen.

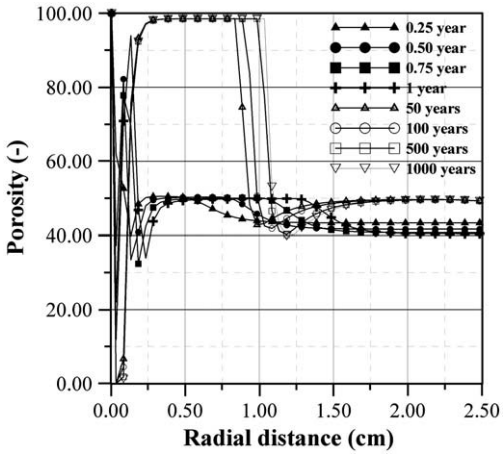

Fig. 12. Evolution of porosity with time for the Standard 5/5 injection grout specimen.

Given that the availability of bicarbonates precludes the formation of a calcite layer, the core of the grout specimen cannot be preserved from the exposure to groundwater, and calcium-containing mineral phases are steadily degraded. In this manner, it can be concluded that the service life of grout is intimately linked to the precipitation of calcite on the surface.

6. Conclusions

A new methodological approach to a rational study of the optimum mix design for injection grout was presented. Although not intended to dissipate the uncertainties connected to the actual evolution of the process of hydration under field conditions, the method is, in fact, useful with views to define reasonable starting points for modelling of degradation. In turn, reactive transport models would provide insight into the performance of the mixtures analyzed in the long-term and guide the pursuit in a practical and effective manner.

The microstructure of the hardened paste was simulated by digital-image-based algorithms, on the basis of typical mix designs. Simulated microstructures have been linked to reactive solute transport models to evaluate the durability of two different types of cement-based grout in contact with granitic groundwater.

Results of the microstructure simulations match the characteristic properties expected from injection grout. Computed microstructures display a high degree of hydration, high porosity (i.e., between 40% and 60%), low contents of aluminium compounds, (including nil amounts of ettringite and hydrogarnet) and, for the P308B grout, low contents of portlandite due to the addition of silica fume. Furthermore, the pH of the pore solution in equilibrium with the solid phases in that case (P308B grout), obtained by means of geochemical speciation, is in the range of typical low-pH cements.

The reactive transport model was aimed at evaluating the degradation of a long drill hole for grout injection surrounded by a relatively thick layer of highly porous granite, and immersed in seawater.

Simulations were carried out for the two mix designs considered and for a boundary water with a chemical composition typical of the Laxemar area (Sweden) at the projected depth of a repository for nuclear spent fuel. They were repeated for a different water in which the content of bicarbonates was reduced by one order of magnitude.

The results obtained show that the process of deterioration is related to two main phenomena, namely, the decalcification of mineral phases (which involves the depletion of portlandite, when

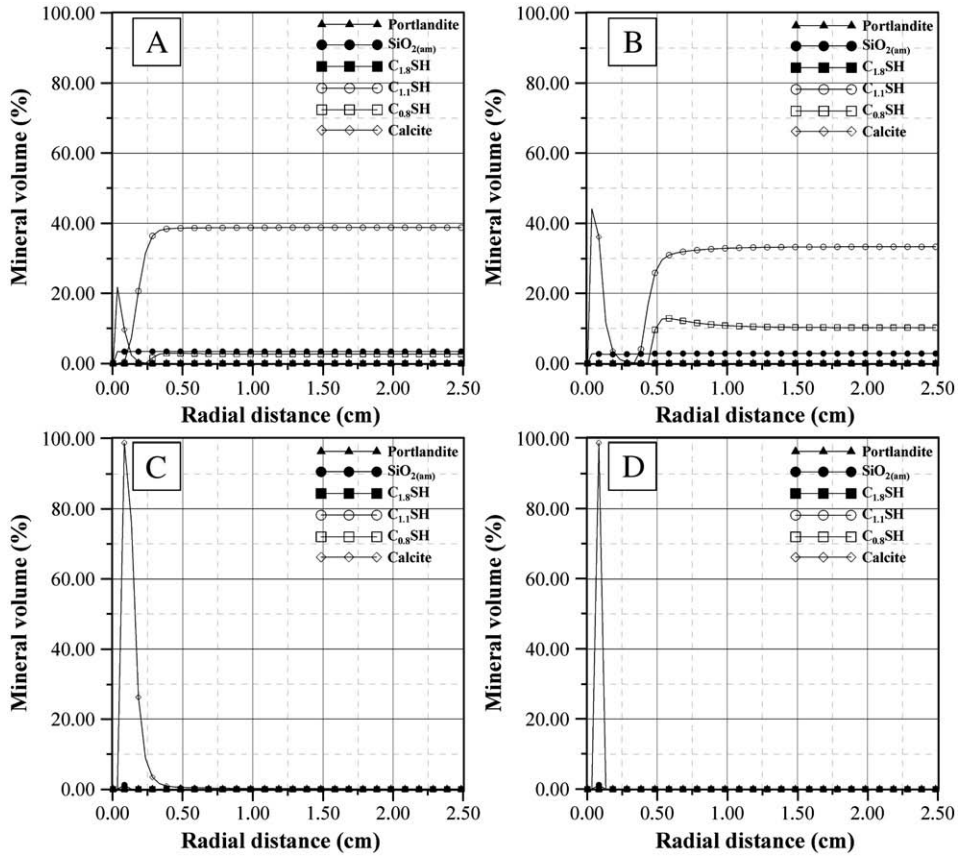

Fig. 13. Mineral constitution of P308B injection grout after (A) 0.25 year, (B) 1 year, (C) 50 years and (D) 100 years.

available) and the precipitation of calcite. It is seen that, under the exposure of typical Laxemar groundwater, the durability of both grout mixes will be guaranteed for thousands of years. However, the sensitivity analysis shows that groundwaters with low bicarbonate concentrations could accelerate dramatically the degradation process, this effect being related to the absence of calcite precipitation.

Acknowledgments

This work has been carried out within the framework of a Research Project (DECON Project) funded by the Swedish Nuclear Fuel and Waste Management Company (SKB). Thanks are especially given to Ignasi Puigdomenech for his support, encouragement and suggestions. The authors would also like to acknowledge the constructive comments of two anonymous reviewers which have contributed significantly to improve the original manuscript.

References

[1] A. Bodén, U. Sievänen, Low-pH injection grout for deep repositories, Summary Report from a Co-operation Project between NUMO (Japan), Posiva (Finland) and SKB (Sweden), R-05-40, 2005.
[2] L. Trotignon, H. Peycelon, X. Bourbon, Comparison of performance of concrete barriers in a clayey geological medium, Phys. Chem. Earth 31 (2006) 610–617.
[3] V. Matte, M. Moranville, F. Adenot, C. Richet, J.M. Torrenti, Simulated microstructure and transport properties of ultra-high performance cement-based materials, Cem. Concr. Res. 30 (2000) 1947–1954.
[4] J. Marchand, D.P. Bentz, E. Samson, Y. Maltais, Influence of Calcium Hydroxide Dissolution on the Transport Properties of Hydrated Cement Systems, Reactions of Calcium Hydroxide in Concrete, American Ceramic Society, Westerville, USA, 2001.
[5] M. Moranville, S. Kamali, E. Guillon, Physicochemical equilibria of cement-based materials in aggressive environments—experiment and modeling, Cem. Concr. Res. 34 (2004) 1569–1578.
[6] E. Holt, Durability of Low-pH Injection Grout — A Literature Survey, Posiva Oy working report 2006-XX, 2006.
[7] A. Kronlöf, Injection grout for deep repositories — low-pH cementitious grout for large fractures: Testing technical performance of materials. VTT Building and Transport, Posiva working report 2004–45, 2004.
[8] U. Sievänen, P. Syrjänen, S. Ranta-aho, Injection grout for deep repositories — low-pH cementitious grout for larger fractures: field testing in Finland, pilot tests. Posiva working report 2004–47, 2005.
[9] D.P. Bentz, P.V. Coveney, E.J. Garboczi, M.F. Kleyn, P.E. Stutzman, Cellular automaton simulations of cement hydration and microstructure development, Model. Simul. Mat. Sci. Eng. 2 (1994) 783–808.
[10] D.P. Bentz, Three-dimensional computer simulation of cement hydration and microstructure development, J. Am. Ceram. Soc. 80 (1) (1997) 3–21.
[11] D.P. Bentz, C.J. Haecker, An argument for using coarse cements in high performance concretes, Cem. Concr. Res. 29 (1999) 615–618.
[12] D.P. Bentz, E.J. Garboczi, C.J. Haecker, O.M. Jensen, Effects of cement particle size distribution on performance properties of cement-based materials, Cem. Concr. Res. 29 (1999) 1663–1671.
[13] D.P. Bentz, O.M. Jensen, K.K. Hansen, J.F. Olesen, H. Stang, C.J. Haecker, Influence of cement particle size distribution on early age autogenous strains and stresses in cement-based materials, J. Am. Ceram. Soc. 84 (1) (2000) 129–135.
[14] D.P. Bentz, X. Feng, C.J. Haecker, P.E. Stutzman, Analysis of CCRL Proficiency Cements 135 and 136 Using CEMHYD3D, NISTIR 6545, U.S. Department of Commerce, 2000.
[15] D.P. Bentz, J.T. Conway, Computer modeling of the replacement of "coarse" cement particles by inert fillers in low w/c ratio concretes: Hydration and strength, Cem. Concr. Res. 31 (2001) 503–506.
[16] J.W. Bullard, User's Guide to the Virtual Cement and Concrete Testing Laboratory Version 1.1 (2000). Available online at http://vcctl.cbt.nist.gov/vcctl/vcctl11/master.html.
[17] D.P. Bentz, P.E. Stutzman, SEM/X-ray imaging of cement-based materials, in: H.S. Pietersen, J.A. Larbi, H.H.A. Janssen (Eds.), Proceedings of the 7th Euroseminar on Microscopy Applied to Building Materials, 1999, pp. 457–466.
[18] J.J. Chen, J.J. Thomas, H.F.W. Taylor, H.M. Jennings, Solubility and structure of calcium silicate hydrate, Cem. Concr. Res. 34 (2004) 1499–1519.
[19] J.M. Galíndez, Coupled water flow and reactive transport modeling and its application to the simulation of cement degradation processes, Master thesis, Universidade de Santiago de Compostela, Spain, 2006.
[20] E. Guillon, Durabilité des matériaux cimentaires. Modélisation de l'influence des équilibres physico-chimiques sur la microstructure et les propriétés mécaniques résiduelles, PhD Thesis, École Normale Supériere de Cachan, France, 2004.
[21] R. Barbarulo, J. Marchand, K.A. Snyder, S. Prene, Dimensional analysis of ionic transport problems in hydrated cement systems Part 1. Theoretical considerations, Cem. Concr. Res. 30 (2000) 1955–1960.
[22] J. Bear, Y. Bachmat, Introduction to Modeling of Transport Phenomena in Porous Media, Kluwer Academic Publishing, Dordrecht, The Netherlands, 1991.

[23] D.P. Bentz, CEMHYD3D: A Three-Dimensional Cement Hydration and Microstructure Development Modeling Package. Version 2.0, NISTIR 6485, U.S. Department of Commerce, 2000.
[24] M. Laaksoharju, Hydrogeochemical evaluation. Preliminary site description Laxemar subarea — version 2.1, SKB Report R-06-70, 2006. Available online at http://www.skb.se/upload/publications/pdf/R-06-70webbNY.pdf.
[25] S.A. Stronach, F.P. Glasser, Modelling the impact of abundant geochemical components on phase stability and solubility of the CaO–SiO2–H2O system at 25 °C: Na+, K+, SO42−, Cl − and CO32−, Adv. Cem. Res. 9 (1997) 167–181.
[26] J.C. Westall, J.L. Zachary, F.M. Morel, MINEQL — A Computer Program for the Calculation of Chemical Equilibrium Composition of Aqueous Systems, Massachusetts Institute of Technology, Cambridge, USA, 1976.
[27] C.I. Steefel, S.B. Yabusaki, OS3D/GIMRT, Software for Multicomponent–Multidimensional Reactive Transport: User's Manual and Programmer's Guide, PNL–11166, Pacific Northwest National Laboratory, Richland, Washington, USA, 1996.
[28] C.I. Steefel, GIMRT, Version 1.2: Software for Modeling Multicomponent, Multidimensional Reactive Transport. User's Guide, UCRL-MA-143182, Lawrence Livermore National Laboratory, Livermore, USA, 2001.
[29] C.I. Steefel, CrunchFlow - Software for Modeling multicomponent reactive flow and transport, Lawrence Berkeley National Laboratory, 2008. Available online at http://www.csteefel.com/CrunchPublic/CrunchFlowManual.pdf.
[30] G.E. Archie, The electrical resistivity log as an aid to determining some reservoir characteristics, Trans. Am. Inst. Min. Eng. 146 (1942) 54–61.
[31] E.J. Garboczi, D.P. Bentz, Computer simulation of the diffusivity of cement-based materials, J. Mater. Sci. 27 (1992) 2083–2092.
[32] C. Carde, R. François, J.M. Torrenti, Leaching of both calcium hydroxide and C–S–H from the cement paste: modeling the mechanical behavior, Cem. Concr. Res. 26 (1996) 1257–1268.
[33] P. Faucon, F. Adenot, J.F. Jacquinot, J.C. Petit, R. Cabrillac, M. Jorda, Long-term behaviour of cement pastes used for nuclear waste disposal: review of physico-chemical mechanisms of water degradation, Cem. Concr. Res. 28 (1998) 847–857.
[34] B. Lagerblad, Leaching Performance of Concrete Based on Studies of Samples from Old Concrete Constructions, SKB Technical Report TR-01-27, 2001.
[35] T. Van Gerven, D. Van Baelen, V. Dutré, C. Vandecasteele, Influence of carbonation and carbonation methods on leaching of metals from mortars, Cem. Concr. Res. 34 (1) (2004) 149–156.